The Evolution of Spin Bags from Small to Large U: Implications for Spectroscopies

A.P. Kampf

J.R. Schrieffer

Department of Physics
University of California
Santa Barbara CA 93106

Abstract: The parent compounds of high temperature oxide superconductors are antiferromagnetic. The nature of hole excitations in the parent compounds is discussed in both the weak coupling or spin density wave (SDW) regime and the strong coupling, or t-J model limit. One finds that the hole becomes dressed by a cloud of antiferromagnetic spin fluctuations which describe the reduction of the staggered antiferromagnetic order parameter in the vicinity of the hole. In addition a twist of the spin quantization axis occurs near the hole. As the hole concentration x increases, long range antiferromagnetic order is suppressed with finite range spin fluctuations occuring in the superconducting phase. The nature of the hole-like excitations in this regime is discussed. One finds that as in the ordered antiferromagnetic regime, the one particle spectral function is dominated by two peaks centered near the SDW or Mott Hubbard upper and lower bands. In addition, there appears a third peak of fundamental importance in understanding the position of the chemical potential as a function of doping. This peak located between the upper and lower bands corresponds to a fully dressed quasi particle with very small weight z_k which is populated by doping and can be probed by photoemission spectroscopy. This split off band removes spectral weight from both the lower and upper bands and leads to a foot on the photoemission intensity versus binding energy curve as seen experimentally. For increased doping the spin fluctuations are reduced in amplitude as the spin-spin correlation length becomes of order the atomic spacing. In this regime the Landau quasiparticle scheme is restored. It is argued that the spin bags or polarons evolve smoothly from the weak coupling SDW to the strong coupling large U regime as do the corresponding spectra.

Keywords: High T_c superconductivity, photoemission spectroscopy, spin density wave, spin bag, spin polaron.

I. INTRODUCTION

Current theoretical efforts to understand high temperature superconducting material can be classified into two categories, namely novel and exotic. In novel approaches a pairing type condensation is assumed to exist with fermion quasi particles of charge $\pm e$ and s $= \frac{1}{2}$ being paired by an effective attractive interaction, with superconductivity already latent in a two dimensional copper oxide plane and phase fluctuations being suppressed when interplanar hopping extends the pairing correlations to three dimensions.

In exotic approaches, many if not all of these conditions are violated. For example, in the resonating valence bond and related approaches, the excitations are taken to have charge $\pm e$ and spin 0 (holon) and charge 0 and spin one-half (spinon). Thus, it is presumed that for the doped material in the absence of long range antiferromagnetic order, an injected hole spontaneously fissions into a holon and spinon, the presumed stable excitations. While at first sight such a spontaneous decay appears peculiar, similar effects actually occur in quasi one-dimensional conductors such as polyacetylene where the excitations are charged spinless solitons and neutral spin one-half solitons. The statistics of such excitations depends on the theoretical framework being used. So-called anyon statistics implies that the ground state of the system breaks time reversal symmetry as in the ground state of the quantum Hall effect where an external magnetic field B_0 is imposed. In high T_c materials a spontaneously broken time reversal symmetry is assumed although the existence of a ground state having such broken symmetry has yet to be demonstrated either experimentally or theoretically starting from a credible Hamiltonian. It is well known that one can transmute the statistics of particles in two dimensions by attaching statistical flux tubes to the particles. Thus, anyons can be transformed to a bosonic or fermionic representation with a suitable interaction between the statistical flux tubes being included. Most of these exotic schemes require at least weak three dimensional coupling for superconductivity to occur.

While the two categories of theories appear to be exceedingly different, there are certain common features between them. The first such feature is the fact that the quasiparticle renormalization constant z_k is small compared to unity. That is, the amplitude for a bare hole to be inserted in a fully dressed state is small compared to one. This feature occurs not only in the two schemes mentioned above but also in the so-called marginal Fermi liquid[1] approach in which the hole self energy exhibits anomalous behavior near the chemical potential.

A second common feature is the strong correlations leading to non-Fermi liquid temperature and energy dependence in the normal state which occurs in both limiting approaches. Such anomalous normal state properties are dictated by experiment. What is less clear is which of the approaches to the superconducting phase will ultimately be correct. Recent experiments probing the broken time reversal symmetry of the superconducting phase suggest evidence both pro and con. We must await the final experimental resolution to this fascinating question.

The generic phase diagram of high temperature superconductors is shown in Figure 1a.

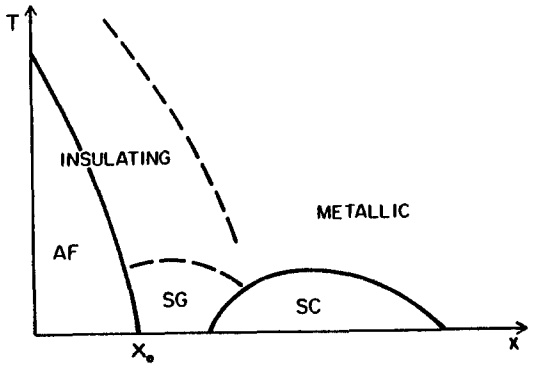

Figure 1a. Phase diagram of high T_c materials of doping x.

For weak doping the system is an antiferromagnetic insulator with the Néel temperature vanishing at a concentration x_0 which is typically of order 3% holes. The smallness of x_0 indicates that the magnetic form factor of a dressed hole involves the suppression of antiferromagnetism in a significant region surrounding the hole encompassing of order 10 neighboring sites. This picture is consistent with the fact that long range antiferromagnetic order in such an anisotropic antiferromagnet continues only to small hole concentrations. For doping larger than x_0 a spin glass-type phase appears in which the dressed holes are likely pinned to charged impurities, perhaps in the fashion of weak localization. For larger doping, this glass melts and the semiconducting behavior of the spin glass converts into metallic behavior leading to superconductivity. In this regime, one is dealing with a strongly correlated system or a "strange metal". Finally, as the doping continues, the system presumably approaches Fermi liquid behavior although thermodynamically it is difficult to achieve such large dopings in a stable materials.

Figure 1b shows a schematic density of states as a function of energy for each of the principal regimes–the antiferromagnetic insulator, the strongly correlated metal and the paramagnetic Fermi liquid.

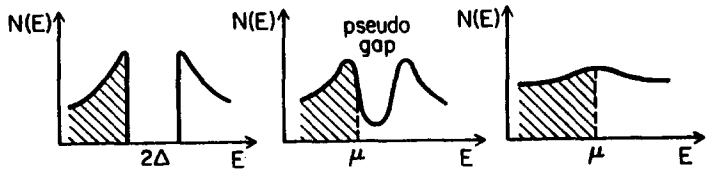

Figure 1b. A schematic density of electronic states for the antiferromagnetic, pseudogap and Fermi liquid regimes.

One sees that the gap characteristic of the antiferromagnetic insulator is transformed into a pseudogap in the strange metal phase and finally a bump characteristic of a mass enhancement in the Fermi liquid regime. The principal theoretical puzzle is to understand the normal phase of this strange metal and how the peculiar excitations in this regime lead to high T_c superconductivity.

II. THE HUBBARD MODEL

The essential physics of cuprate superconductors is centered on transport in the two dimensional CuO_2 planes. As mentioned above, phase fluctuations of the superconducting order parameter are quenched by hopping along the direction c perpendicular to the ab planes. Since there are three important orbitals per copper oxides unit cell, namely the copper $d_{x^2-y^2}$ and p_σ for each of the two oxygen atoms, there are three bands important for the spectroscopic properties of these materials. However, since the lower two bands are filled and the upper band is half empty for the parent antiferromagnetic insulator, it is likely that the dominant low energy effects essential for superconductivity can be mapped into a one-band problem in which the copper d orbital and the oxygen p_σ orbitals mix to form an antibonding, partly filled band. It is this upper antibonding band which we consider in an effective two dimensional one band Hubbard model. Interband transitions are, no doubt, important for optical spectra.

The one band Hubbard model is defined by the Hamiltonian

$$H = -t \sum_{\substack{<ij> \\ \sigma}} (c^+_{i\sigma} c_{j\sigma} + h.c.) + U \sum_i n_{i\uparrow} n_{i\downarrow}, \tag{1}$$

In Figure 2a, the mean field Néel temperature T_N is sketched as a function of the coupling constant $g \equiv U/4t$.

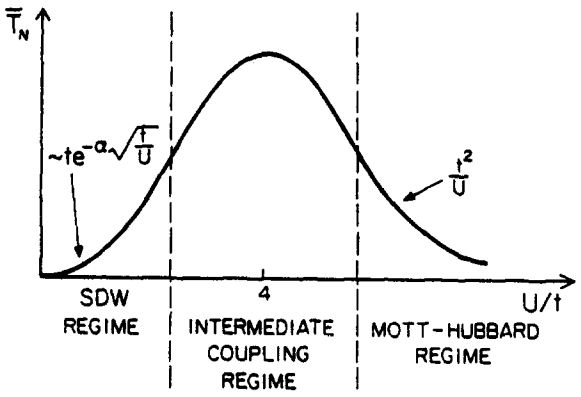

Figure 2a. Mean field Néel temperature versus U/t.

The Néel temperature peaks for g of order unity, with T_N vanishing for both large and small values of g. The region g small compared to unity corresponds to the spin density wave or weak coupling behavior while, g large compared to unity corresponds to the Mott Hubbard strong coupling regime. Experimental evidence suggests that physical reality in the cuprate superconductors occurs for intermediate coupling, with g of order unity.

In Figure 2b the density of $\uparrow$ spin (dashed line) and $\downarrow$ spin (solid line) is shown for the three regimes.

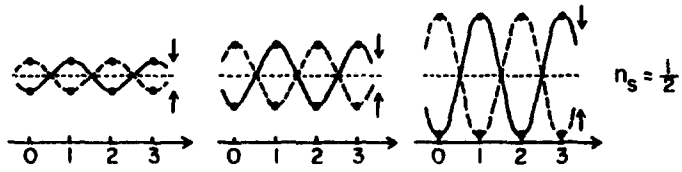

Figure 2b. Density of spin up (dashed line) and spin down (solid line) electrons in the weak, intermediate and strong coupling regimes.

For g of order unity the $\uparrow$ spin tends to sit mainly on the even sites while the down spin sits primarily on the odd sites, although there are fluctuations to the opposite spin configuration. For weak coupling, scattering of electrons by the oscillating exchange potential set up by the spin density wave leads to an energy gap 2Δ. This gap grows as the amplitude of the spin density wave increases and saturates at the value U for large values of g. It is important to note that the gap essentially disappears well above the Néel temperature for weak coupling while it remains essentially U in the strong coupling regime. One can view the persistence of the gap in the spin disordered regime either as a local Coulomb correlation effect or equally well as a local exchange interaction set up by the local moments on the individual sites. These two views are related by a simple mathematical identity

$$Un_{i\uparrow}n_{i\downarrow} = \frac{-U}{2}(n_{i\uparrow} - n_{i\downarrow})^2 + \frac{U}{2}(n_{i\uparrow} + n_{i\downarrow}), \tag{2}$$

We first consider the weak coupling approach for small doping[2]. The sublattice magnetization M_z is shown in Figure 3 as a function of g.

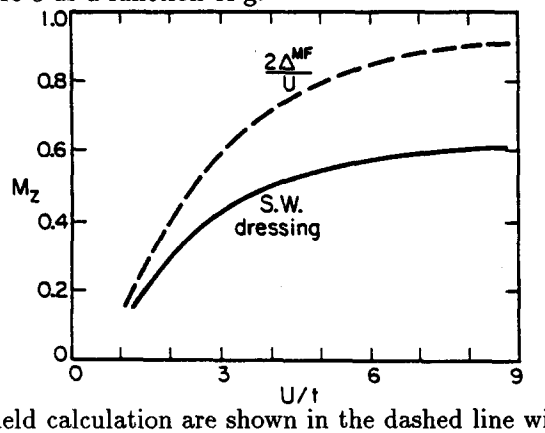

Figure 3. Sublattice magnetization as a function of U/t in the mean field approximation (dashed line) and with gaussian spin fluctuation dressing of the ground state (solid line).

The results of the mean field calculation are shown in the dashed line with the reduction of the sublattice magnetization due to Gaussian spin fluctuations as indicated by the solid line. In Figure 4, the spin wave velocity in units of ta is shown, where a is the lattice spacing.

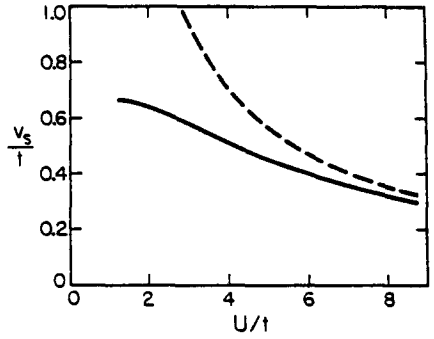

Figure 4. Spin wave velocity for harmonic spin waves about the mean field SDW state (solid line) and the result of the 2-d Heisenberg model with $J = 4t^2/U$.

The solid line indicates the results of mean field plus Gaussian spin wave dressing while the dashed line indicates the results of the antiferromagnetic Heisenberg model. Interestingly, the mean field result reduces to Anderson's result for the Heisenberg model in the large U limit in the absence of spin fluctuation corrections. Thus it appears that the mean field plus Gaussian spin fluctuation approximation gives a reasonable account of the undoped antiferromagnet over the entire coupling constant domain.

III. Fermion Excitations

As shown in Figure 5, for $U = 0$ the electronic spectrum is given by

$$\varepsilon_k = -2t(\cos\ k_x a + \cos\ k_y a). \tag{3}$$

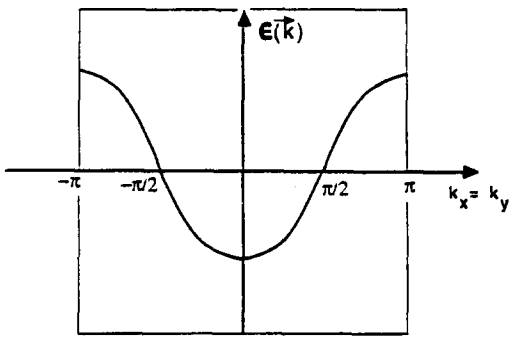

Figure 5. The Bloch energy ε_k for $k_x = k_y$.

In the presence of the spin density wave, exchange Bragg scattering leads to a gap 2Δ in the

spectrum with the energies $E_{\mathbf{k}}$ being

$$E_{\mathbf{k}} = \pm\sqrt{\varepsilon_k{}^2 + \Delta^2}, \tag{4}$$

as shown in Figure 6a.

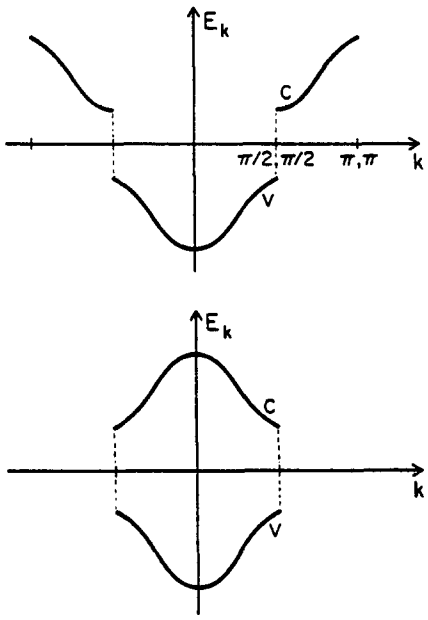

Figure 6a. The mean field SDW Bloch energy ε_k in the full zone (top panel) and in the magnetic (reduced) zone (lower panel).

Electronic states can be described either in the original Brillouin zone or in the magnetic zone where the upper band is folded back into this smaller zone, indicated by the shaded portion of Figure 6b.

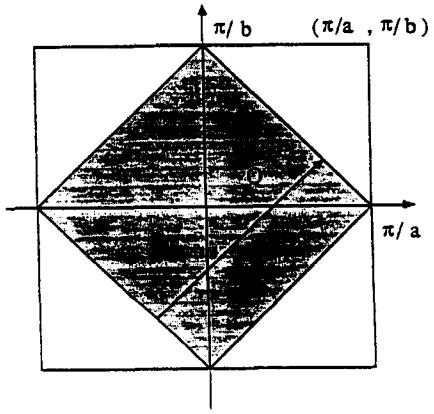

Figure 6b. The full zone and the magnetic zone, illustrating the nesting vector Q.

The quasiparticle operator γ_k creating its mean field excitations is given by

$$\gamma_{ks} = u_k c_{ks} + s v_k c_{k+Q,s}, \tag{5}$$

where $\mathbf{Q}$ is the SDW wave vector $(\pi/a, \pi/a)$. In the undoped antiferromagnetic insulator, the lower band is fully occupied while the upper band is empty. In the large U limit the two bands go over to the lower and upper Mott Hubbard bands. In actuality, an added electron or hole locally weakens antiferromagnetism and leads to a dressing of the fermion with a cloud of spin fluctuations. The dressed excitation, a spin bag or one band polaron, is illustrated in Figure 7 where the staggered magnetization

$$\vec{M}_n = < \vec{S}_n > \cos \vec{Q} \cdot \vec{R}_n, \tag{6}$$

is reduced in magnitude within a region of size ξ_{SDW} defined by

$$\xi_{SDW} = \hbar v_F / \pi \Delta_{SDW}. \tag{7}$$

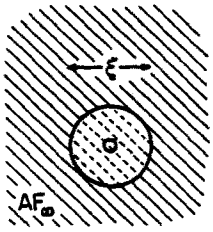

Figure 7. Reduction of the staggered magnetization within the spin bag of size ξ.

The hole self energy $\Sigma_s(\mathbf{k}, \omega)$ is shown within the one loop approximation in Figure 8.

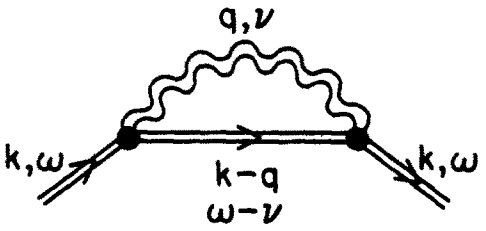

Figure 8. Hole self energy, where the fermion propagator and the vertices represent γ particles, Eqn. (5), and the boson is the RPA spin wave, both longitudinal and transverse modes.

Notice that both the fermion and boson line are excitations within the mean field SDW approximation with coherence factors entering at the vertices. The boson line is the longitudinal or transverse spin susceptibility for the SDW. χ^{zz} leads to the reduction of M_z within the bag while $\chi^{\pm}$ creates the spin twist about the bag with the spacial variation given by an inverse power law falloff. The spin bag is analogous to the polaron in a semiconductor where the band gap is locally reduced in the presence of an added electron or hole.

When two holes are added the interaction is given to leading order by the exchange of one dressed spin fluctuation as indicated in Figure 9a.

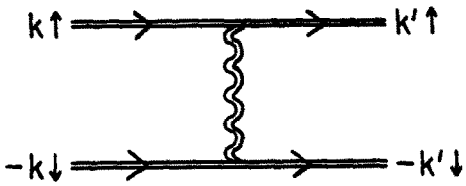

Figure 9a. The pairing interaction between γ states within the one spin wave approximation.

The pairing potential $V_{\mathbf{k}\mathbf{k}'}$ within this approximation is shown in Figure 9b.

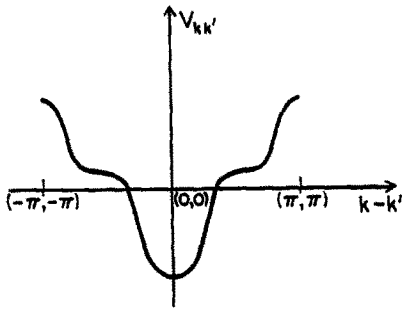

Figure 9b. Pairing potential for the graph of Figure 9a.

These result first derived by Wen, Zhang and one of the authors shows a region of strong attraction for momentum transfers $\mathbf{k} - \mathbf{k}'$ smaller than the inverse bag size. This is in sharp contrast with the Born approximation for bare particles interacting with bare phonons as shown in Figure 10 with V being repulsive for all values of $\mathbf{k} - \mathbf{k}'$. Therefore, the bag effect is essential to obtain an attractive interaction in this system.

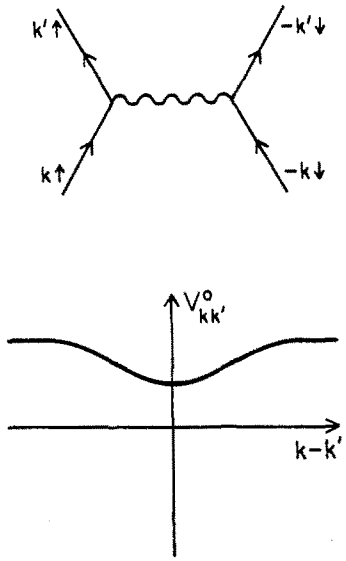

Figure 10. Pairing interaction diagram between bare Bloch electrons c_k (upper panel), illustrating that the potential is repulsive in this approximation for all $k - k'$.

IV. Intermediate Doping and Short Range Spin Correlations

We next consider the doping range x corresponding to a strongly correlated metal as shown in Figure 1. This regime can be approached from the large x regime where Fermi liquid theory presumably holds. On reducing x, antiferromagnetic spin fluctuations build up, both in amplitude and in spatial coherence with the spin-spin correlation length eventually diverging as one approaches the antiferromagnetic insulator instability. Kampf and Schrieffer[3] have explored this regime by considering the one particle self energy $\Sigma_s(\mathbf{k}, \omega)$ as illustrated in Figure 11 within the one loop approximation.

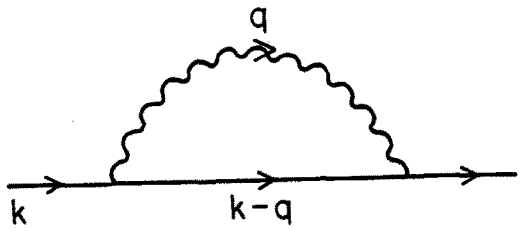

Figure 11. One loop self energy in the paramagnetic regime. The spin wave is summed over longitudinal and transverse modes.

The boson propagator was represented by the susceptibility

$$\chi(\mathbf{q}, \omega) = \lambda^2 \sum_{Q} \frac{\Gamma}{(\mathbf{q} - \mathbf{Q})^2 + \Gamma^2} F(\omega), \tag{8}$$

where Γ is the reciprocal of the spin-spin correlation length and $F(\omega)$ is given by

$$F(\omega) = \int \frac{2\nu g(\nu)\, d\nu}{\omega^2 - \nu^2 + i\delta}, \tag{9a}$$

$$g(\nu) = \begin{cases} \alpha \mid \nu \mid, \mid \nu \mid < \omega_o \\ 0, \quad otherwise. \end{cases} \tag{9b}$$

This form is similar to that used by Millis, Monien, and Pines[4]

$$\chi_{AF}(\mathbf{q},\omega) = \frac{\chi \mathbf{Q}}{1 + (\mathbf{Q} - \mathbf{q})^2 \xi^2 - i \cdot \frac{\omega}{\omega_{SF}}}, \tag{10}$$

For large doping the spin-spin correlation length is very short and one obtains a self energy of the form shown in Figure 12.

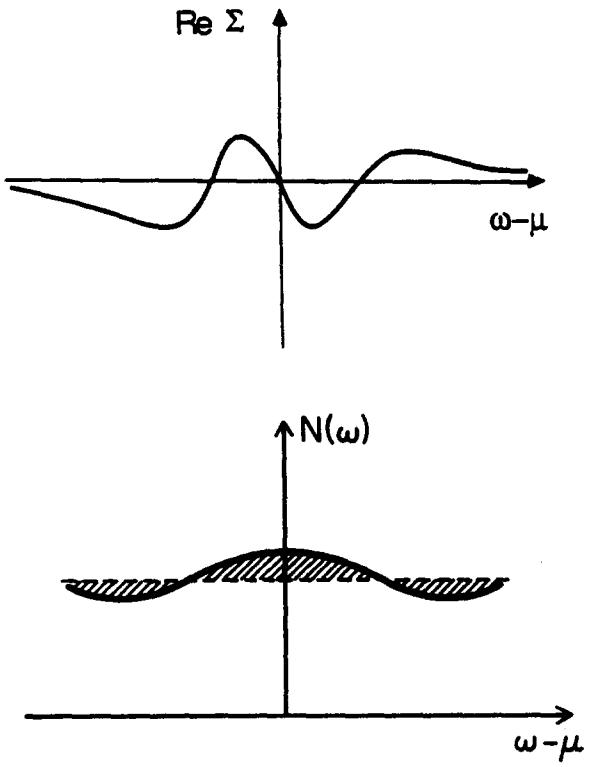

Figure 12. The real part of the electron self energy $Re\Sigma$ in the Fermi liquid regime (top panel) and the corresponding density of states enhancement at the chemical potential, corresponding to $m^t / m > 1$.

An essential point is that in this regime the slope of Σ as a function of ω is negative over a substantial region around the Fermi surface. This leads to an increase of the density of states near the Fermi surface and a depletion away from the Fermi surface.

This conventional Fermi liquid picture is drastically altered when the spin-spin correlation length becomes large compared to the interatomic spacing. In this case, the real part of Σ takes on a very different form as shown in Figure 13a.

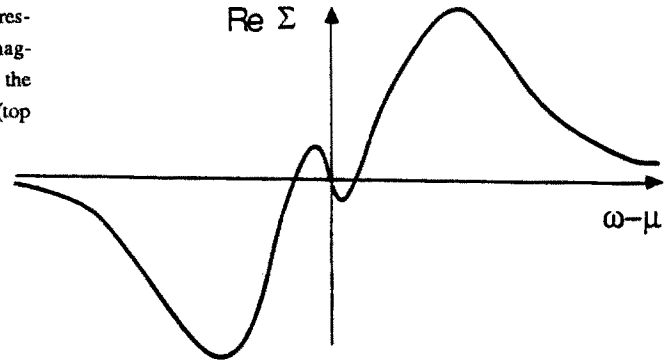

Figure 13a. *Re*Σ in the presence of strong antiferromagnetic spin fluctuations in the paramagnetic phase (top panel).

Except for the small wiggle near the chemical potential, the basic slope of Σ is positive rather than negative. Thus, since the real part of Σ corresponds to the level shift effect, states of positive energy are pushed up and states of negative energy are pushed down leading to a pseudo gap indicated in Figure 13b.

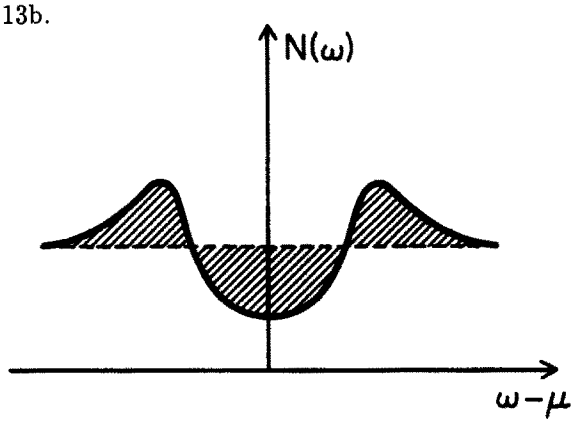

Figure 13b. The formation of a pseudo gap.

The physical origin of these two quite different energy dependences of Σ can be understood as follows: two possible time orderings of the vertices in Fig. 11 can occur. In Figure 14a one has the conventional polaron self energy in which an injected hole is scattered into an intermediate hole state beneath the Fermi surface, as for a hole polaron in a semiconductor.

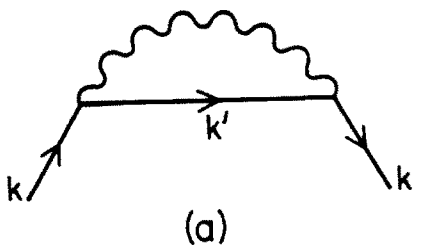

Figure 14a. Polaron time ordering of the self energy graph, in which a hole occupies the intermediate state k'.

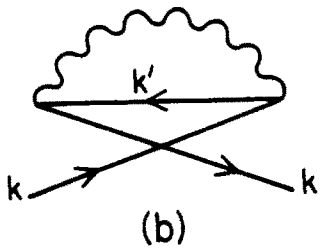

Figure 14b. The exchange graph which describes the Pauli principle suppression of a spin fluctuation process which lowers the system energy in the absence of the added hole. Thus, this contribution raises the hole (and the k electron) energy and leads to a pseudo gap.

However, as shown in Figure 14b an injected hole can also be converted into an electron above the Fermi surface in the intermediate state. This second diagram physically arises from the suppression of vacuum spin fluctuations by the action of the exclusion principle effect associated with the added hole. This can best be seen as in Figure 15a where the added hole in state k excludes a vacuum fluctuation.

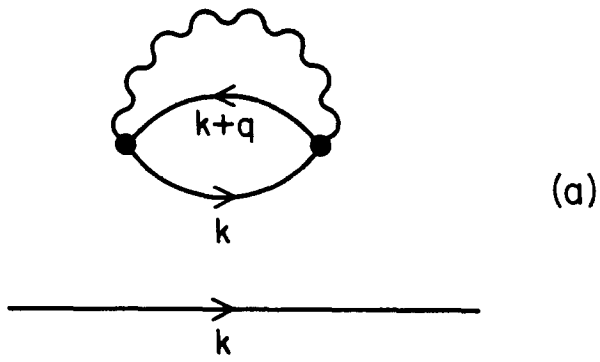

Figure 15a. The vacuum fluctuation referred to in Figure 14b.

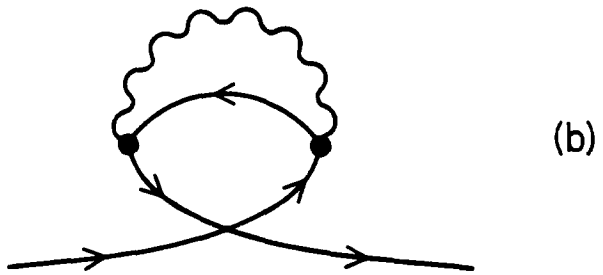

Figure 15b. The Feynman exchange graph essential to preserve the Pauli principle and the linked cluster expansion.

In this state a second hole, also in state k, is contained in the vacuum spin fluctuation and is forbidden by the exclusion principle. As Feynman showed, such Pauli principle violating effects can be handled by adding another diagram given by exchanging the lines of the two violating particles as is shown in Figure 15b. This extra diagram precisely cancels the forbidden graph, and also allows one to preserve the linked cluster expansion which is crucial to the proper volume scaling of the system energy. Since the vacuum fluctuation energy *lowers* the total system energy in the absence of the hole, the introduction of the hole *raises* the energy and therefore leads to the pseudo gap behavior characteristic of Figure 13, recalling that increasing hole energy is measured toward *negative* $\omega - \mu$.

V. Implications for Photoemission Spectroscopy

Photoemission and inverse photoemission spectroscopy in essence measure the one particle spectral function

$$A(\mathbf{k},\omega) = \mid \frac{1}{\pi} ImG(\mathbf{k},\omega) \mid = \mid \frac{1}{\pi} Im \frac{1}{\omega - \varepsilon_{\mathbf{k}} - \Sigma(\mathbf{k},\omega)} \mid . \tag{11}$$

Angular resolved spectra measure both the $\mathbf{k}$ and ω dependence of A, as shown in Figure 16.

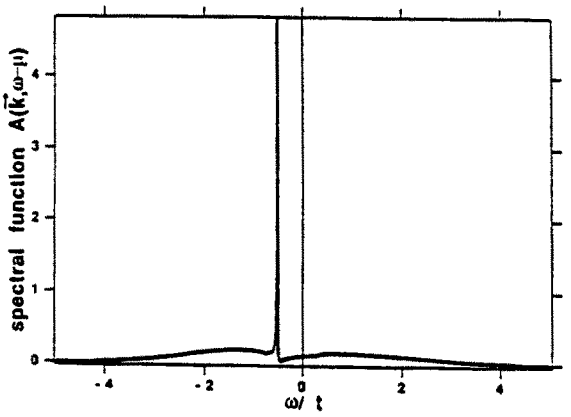

Figure 16. Hole spectral function for spin-spin correlation length $L_{ss} = 1/\Gamma = a$, and $k = 0.9(\pi/2,\pi/2)$. This illustrates Fermi liquid behavior.

In the large doping limit the Landau theory presumably holds with a sharp quasiparticle peak located at the renormalized single particle energy and two incoherent peaks, one for holes and the other for electrons occurring at large energy. As the doping is reduced the spin-spin correlation length grows and the weight of the quasiparticle z_k is reduced, with the incoherent backgrounds becoming more sharply defined, as shown in Figure 17.

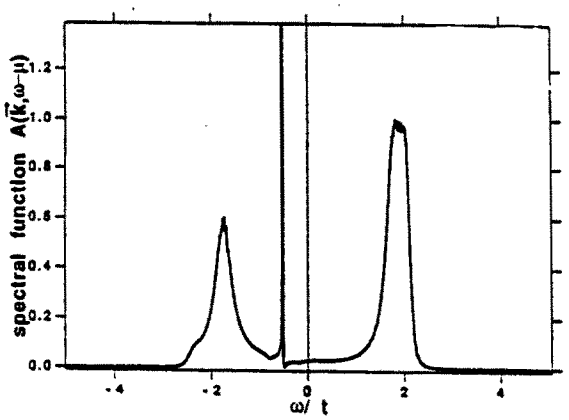

Figure 17. Hole spectral function for $L_{ss} = 20a$ and $k = 1.15(\pi/2,\pi/2)$ illustrating sharpening of the incoherent backgrounds which arise from quasi-Bragg scattering of the hole by the large amplitude slow spin fluctuations. The quasi particle amplitude z_k is small.

Finally, in the antiferromagnetic phase, if $\mathbf{k}$ is near the magnetic Brillouin zone boundary, A becomes two sharp peaks as seen in Figure 18.

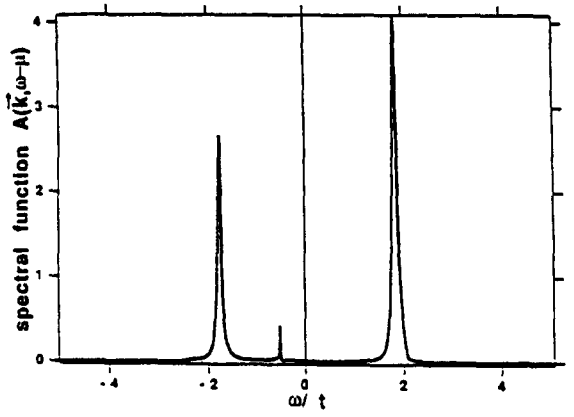

Figure 18. Hole spectral function near the SDW transition, for $L = 100a$. Clearly the quasi particle has extremely small weight and the SDW split peaks appear. The smaller of the two peaks is called the shadow band.

Using the phenomenological model susceptibility and evaluating the spectral function $A(k,\omega)$ for momenta close to the Fermi momentum allows one to follow the Landau quasiparticle peak as it disperses through the Fermi level. Figure 19 shows the corresponding finite temperature photoemission spectrum, very similar in their line shape to the experimental data by Olson, *et al.*[6]

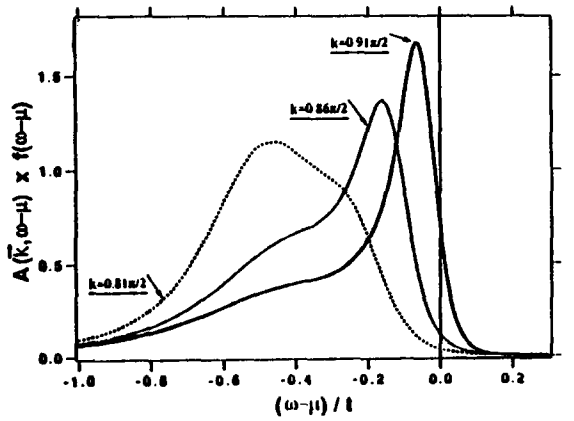

Figure 19. Photoemission spectrum for several values of k near k_F.

For each $\mathbf{k}$ an additional sharp feature appearing in the spectral function in the pseudogap regime should also be observable near momentum $\mathbf{k}+\mathbf{Q}$ where $Q = (\pm\pi, \pm\pi)$ is the antiferromagnetic wave vector. Although there is a unique quasiparticle state for each $\mathbf{k}$ in the reduced magnetic Brillouin zone, the wave function for such a state is a linear combination of Bloch waves for wave vectors $\mathbf{k}$ and $\mathbf{k}+\mathbf{Q}$. Therefore the emitted electron will carry momentum $\mathbf{k}$ as well as $\mathbf{k}+\mathbf{Q}$ even though a single unique quasihole state is created. The spectral intensity associated with the exchange Bragg scattering therefore leads to a shadow band displaced by $\mathbf{Q}$.

An interesting feature in the spectrum has been observed by Allen and coworkers[7] in $Nd_{2-x}Ce_xCuO_{4-y}$. They find that in contrast to a rigid band model, their data are consistent with a picture in which each hole splits off a state from the valence band, thereby pinning the chemical potential inside the gap. It is suggestive that this effect is the result of spin bag formation, which splits one state off from a linear combination of the valence and conduction bands, with weights favoring the band whose edge is nearer the spin bag energy. For large doping, this effect will smear into the band edge, as in heavily doped semiconductors. To treat this effect, it is essential to include in Σ the two loop crossed line diagram. In essence, one loop produces the pseudogap discussed above and the second loop accounts for the local depression of the pseudogap to form a bag. This is in analogy with the situation in the ordered antiferromagnet, where the mean field potential produces the gap and the loop accounts for the depression of the gap in the vicinity of the hole to form the bag. Model calculations of this effect are in progress[8].

VI. The Large $U/4t$ Limit

Many authors have studied both the 2d one band Hubbard model for large U and the t-J model using a variety of techniques, both analytic and numerical. The results are remarkably similar to those discussed above in the weak coupling theory. In particular, bag effects are observed including the spin twist mentioned above.

In addition, the dressed holes are observed to attract as in the weak coupling situation. The one hole spectral weight function $A(k,\omega)$ exhibits a small or vanishing z_{k_F} corresponding to a large incoherent shakeoff spectrum when a hole is created. The reader is referred to the literature concerning such effects[9,10].

Concerning charge and spin separation postulated in the exotic approaches, to date no calculations on the Hubbard, t-J and related models have shown these quantum numbers to be deconfined so that the charge and spin of the excitations are very likely to be the conventional ones for a hole or an electron, namely charge $\pm e$ and spin $\frac{1}{2}$, although the issue remains open at present.

This work was supported in part by NSF grant DMR89-16582 and by the Electric Power Research Institute, contract RP8009-18.

REFERENCES

1 C.M. Varma, et al. Phys.Rev.Lett. 63, 1996 (1989).

2. J.R. Schrieffer, X.-G. Wen, and S.-C. Zhang, Phys.Rev.B. 39, 11663 (1989); Phys.Rev.Lett. 60, 944 (1988).

3. A.P. Kampf and J.R. Schrieffer, Phys.Rev.B. 42, 7969 (1990).

4. A.J. Millis, H. Monien, and D. Pines, Phys.Rev.B. 42, 167 (1990); H. Monien, P. Monthoux, and D. Pines, Phys.Rev.B. 43, 275 (1991).

5. A.P. Kampf and J.R. Schrieffer, Phys.Rev.B. 41, 6399 (1990).

6. C.G. Olson, et al., Phys.Rev.B. 42, 381 (1990).

7. J.W. Allen, et al., Phys.Rev.Lett. 64, 595 (1990).

8. A. Kampf and J.R. Schrieffer, work in progress; see also, C. Melo and S. Doniach, Phys. Rev. B 41a, 6633 (1990).

9. D.J. Scalapino, The Los Alamos Symposium, High Temperature Superconductivity, Addison-Wesley (1990).

10. E. Dagotto, International Journal of Physics B 5, 77 (1991).